PERGAMON

Deep-Sea Research I 47 (2000) 309–322

DEEP-SEA RESEARCH
PART I

Absolutely referenced geostrophic velocity and transport on a section across the North Atlantic Current

Christopher S. Meinen[a,*,1], D. Randolph Watts[a], R. Allyn Clarke[b]

[a]*Graduate School of Oceanography, University of Rhode Island, Narragansett, RI 02882, USA*
[b]*Bedford Institute of Oceanography, Department of Fisheries and Oceans, Dartmouth, NS, B2Y 4A2, Canada*

Received 27 October 1998; received in revised form 2 March 1999; accepted 3 March 1999

Abstract

A transect of CTD profiles crossing the North Atlantic Current (NAC) along WOCE line ACM6 near 42.5°N during August 1–7, 1993, provides geostrophic shear velocity profiles, which were absolutely referenced using simultaneous POGO transport float measurements and velocity measurements from a ship-mounted acoustic doppler current profiler (ADCP). The NAC absolute transport was $112 \pm 23 \times 10^6$ m^3 s^{-1}, which includes a portion of the transport of the Mann Eddy, a large permanent anticyclonic eddy commonly adjacent to the NAC. The NAC transport estimated relative to a level of no motion at the bottom would have underestimated the true total absolute transport by 20%. A surprisingly large 58×10^6 m^3 s^{-1} flowed southward just inshore of the NAC. This flow, centered near 1500 dbars about 200 km offshore of the shelf-break, was fairly barotropic with a peak velocity of greater than 20 cm s^{-1}, and the water mass characteristics were of Labrador Sea Water. These absolute transport observations suggest southward recirculation inshore of the NAC at 42.5°N and a stronger NAC than has previously been observed.

Keywords: North Atlantic current; Absolute transport; Absolute velocity; Acoustic doppler current profiler; ADCP; POGO transport float; CTD

* Corresponding author.
E-mail address: meinen@pmel.noaa.gov (C.S. Meinen)
[1] Current affiliation: Joint Institute for the Study of the Atmosphere and Ocean, University of Washington, Seattle, WA 98115, USA.

0967-0637/99/$ - see front matter
PII: S0967-0637(99)00061-8

1. Introduction

The North Atlantic Current (NAC) has both regional and global impacts. On a global scale, the NAC represents the upper limb of the thermohaline overturning cell (McCartney and Talley, 1982,1984). On a regional scale, the NAC transports warm water farther poleward than any other western boundary current (Rossby, 1996). This moderates the climate for northern Europe, which is warmed by westerly winds crossing these warm waters (Krauss, 1986). Rossby (1996) reviews the evolution of thought on the circulation in the NAC region. Several historical studies have estimated the transport of the NAC at various places along its path. Most have used hydrography and the dynamic method referenced to an assumed "Level of No Motion" (LNM) (Mann, 1967; Mountain and Shuhy, 1980; Clarke et al., 1980; Sy et al., 1992), although a few have involved direct measurements using current meter moorings (Reiniger and Clarke, 1975; Arhan et al., 1989). The well-known problem with the LNM approach is the total lack of information on the barotropic component of the velocity.

This collaborative experiment by the Bedford Institute of Oceanography and the University of Rhode Island determined the absolute transport of the NAC at a location where several historical estimates have been made. A complete hydrographic section was taken across the NAC near 42.5°N. The section involved full-water-column CTDs, hull-mounted acoustic doppler current profiler (ADCP) measurements, and POGO transport float deployments at each of the CTD sites. This paper presents the absolute transports estimated for the NAC as well as the flows inshore and offshore of the NAC.

2. Data

During August 1–7, 1993, a section of 17 full-water-column CTD profiles was taken on a line across the North Atlantic Current 200 km downstream of the Southeast Newfoundland Rise near 42.5°N. The section coincides with WOCE line ACM6. The locations of all the CTD profiles are shown in Fig. 1 in relation to the local bathymetry. At each of the CTD sites, a POGO transport float (Rossby et al., 1991) was also deployed to a depth of about 1000 m (although at one site the POGO failed). The POGO transport float is a glass cylinder just under 2 m in length with a pressure gauge and an acoustic pinger for tracking and distance measuring. The float sinks slowly to a predetermined depth, drops a weight, and rises at nearly the same rate back to the surface. By precisely measuring the location of deployment, the surfacing location, and the intervening time, the mean horizontal velocity between the surface and the maximum depth can be calculated (Rossby et al., 1991). Fig. 2 shows the POGO velocity measurements. In addition to the POGO floats, ADCP measurements were made throughout the section using a hull-mounted RDI 150 kHz ADCP set to collect velocity data in fifty 8-m bins (RDI, 1989). Ship navigation information was provided by GPS for position and speed, by gyrocompass for direction. Based on the quality of the measured ADCP data, the depth range from 50–200 m was chosen

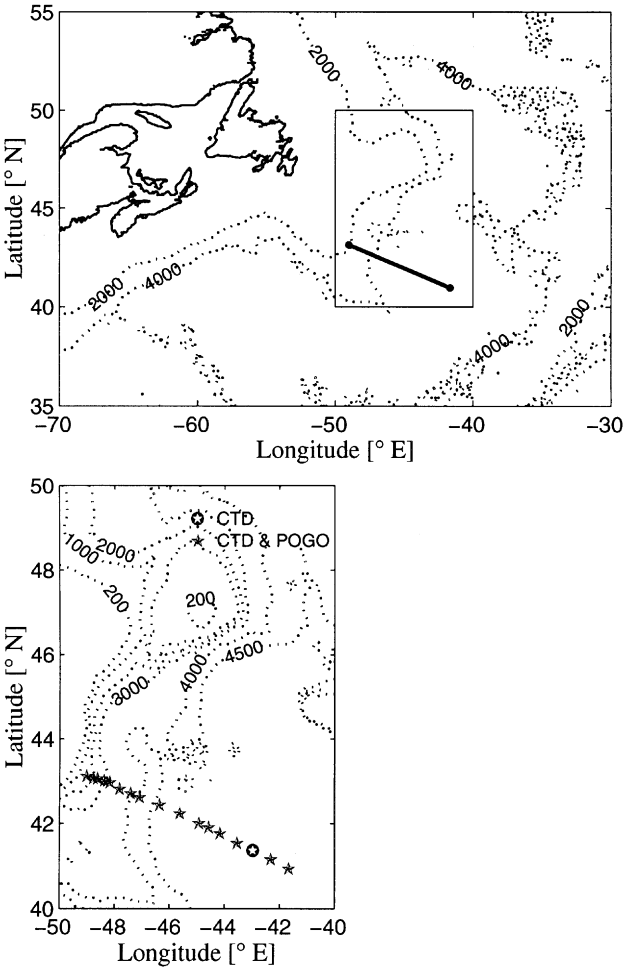

Fig. 1. Upper panel shows study area in relation to the topography of the Newfoundland Basin. The bold line represents our CTD section. Lower panel shows the detailed locations of the CTD sites with POGO transport floats denoted by stars, and the one CTD site where the POGO failed denoted by an open star in a dark circle. The dotted lines indicate bathymetric depth in meters.

as the range where the ADCP consistently provided accurate data throughout the cruise. The velocities were collected as 5 min averages in order to reduce the noise in the measurement. Fig. 3 shows the ADCP measured absolute velocities along the section, where only the measurement taken every 5 h is shown to avoid cluttering the plot.

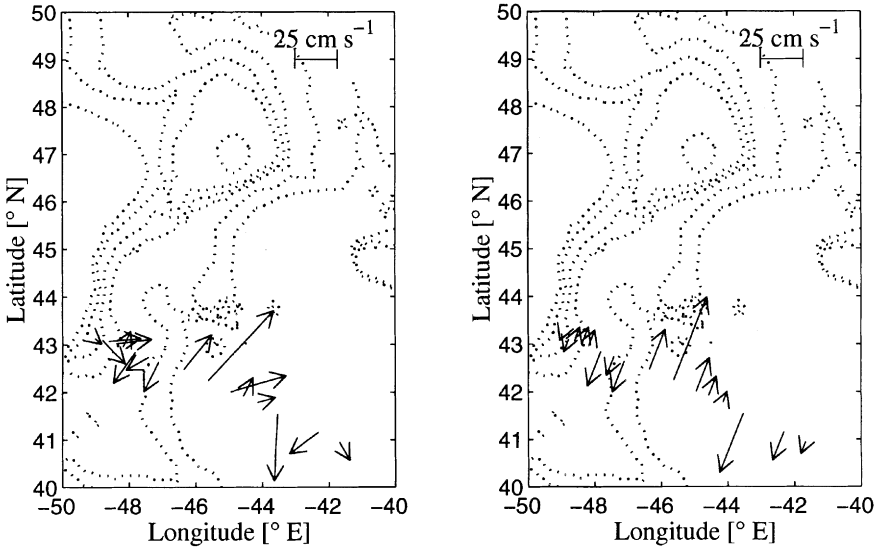

Fig. 2. Velocities averaged over the top $\approx$ 1 km as measured by the POGO transport floats. The panel on the left shows the vector velocities, the panel on the right shows only the component normal to the transect.

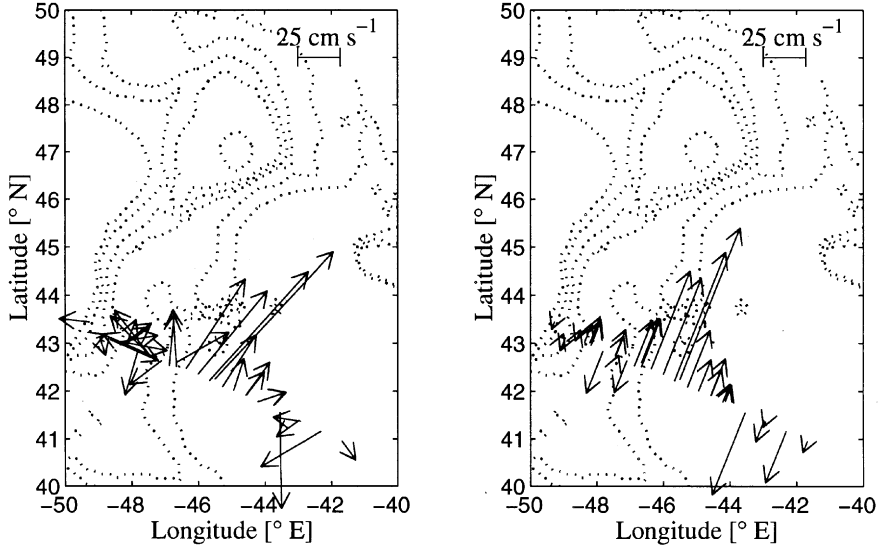

Fig. 3. Five-minute-bin averaged velocities measured by the ADCP. These have been subsampled, showing only the measurements taken every five hours to avoid cluttering the plot. The vectors represent the vertically averaged velocity over 50 to 200 m. The panel on the left shows the vector velocity, the panel on the right shows only the component normal to the transect.

3. Methods

The dynamic method for determining geostrophic velocities using hydrography is well known (Gill, 1982; Fofonoff and Millard, 1983; Pond and Pickard, 1983). The method provides a profile of geostrophic velocity, $V_R(P)$, relative to zero velocity at a reference level P_{ref}. To obtain a profile of absolute geostrophic velocity, this V_R profile must be referenced with an independent, directly measured, absolute geostrophic velocity at any depth, V_{ref}. One problem in referencing geostrophic velocities arises because all methods of measuring the absolute velocity include both geostrophic and ageostrophic components. A second major problem is that most direct velocity measurement systems yield point measurements, while the geostrophic V_R profile represents a horizontal average between the two CTD sites. Oceanic features that are too small to be resolved by the spacing of the CTD casts could have a large impact on point-measured absolute velocities but a small effect on the V_R profiles. Three referencing methods were pursued in this study, building on the methods of Pickart and Lindstrom (1994): using POGO transport floats at the CTD sites (Rossby et al., 1991) using ADCP measurements at the CTD sites, and using ADCP measurements integrated between the CTD sites (Cokelet et al., 1996).

The POGO transport float determines the vertically averaged horizontal velocity between the surface and a predetermined depth (Rossby et al., 1991). The referenced absolute velocity, $V_{absolute}$, is then determined via

$$V_{absolute}(P) = V_R(P) + (V_{pogo} - \langle V_R \rangle), \tag{1}$$

where $\langle V_R \rangle = 1/P_{max} \int_0^{P_{max}} V_R \, dP$, P_{max} is the maximum depth the POGO reaches during the profile, and V_{pogo} is the component of the POGO measured velocity perpendicular to the CTD section. POGO floats were deployed at each CTD site, and the mean of the two POGO horizontal velocities was used to provide the reference, V_{pogo}. Hereafter, this will be referred to as the POGO method.

The ship-mounted ADCP measures water velocity relative to the ship. The ship speed and direction are determined via GPS and gyrocompass, respectively, and this velocity is subtracted from the ADCP-measured velocities to determine absolute water velocities (Pollard and Read, 1989; Saunders and King, 1995). All ADCP velocities have been averaged between 50 and 200 m. The integration limits of $\langle V_R \rangle$ in Eq. (1) are changed to 50 and 200 m and V_{pogo} is replaced by V_{adcp}. Two referencing methods using the ADCP were employed, the first temporally averaged the ADCP profiles obtained while the ship was holding position at the CTD sites, the second spatially integrated the ADCP profiles obtained while steaming between CTD stations (Joyce et al., 1989; Pickart and Lindstrom, 1994; Cokelet et al., 1996). These are referred to as the "ADCP at" and the "ADCP btwn" methods, respectively.

Each of the three referencing methods is subject to a variety of errors, some of which are due to ocean properties, which to a varying degree can affect all three methods, and some of which are method-specific. A detailed discussion of all of the sources of error that were studied is presented in Meinen (1998). The two largest sources of error, regardless of method, are the spatial sampling error and the ageostrophic velocities. The former affects the POGO and "ADCP at" methods but not the "ADCP btwn"

method. For the first two methods only the velocities measured at the CTD sites themselves are used in determining an absolute reference velocity applicable across the whole span between CTD sites; thus any smaller scale velocity structure between CTD sites is not sampled in these two methods. The size of this error for the "ADCP at" method was quantified by first averaging the ADCP data within 2-km-wide bins. Using these 2-km-bin data, mean velocities were obtained by averaging pairs of bins spaced 20 km apart along the whole section. Another set of mean velocities was obtained by spatially integrating the velocities over the same 20-km spacings. The same process was repeated using 40 and 60 km averaging widths. For the "ADCP at" method (vertical average over 50–200 m) the standard deviations of the differences between the 20, 40, and 60 km spaced samples and the spatially integrated means were 3.6, 8.3, and 12.0 cm s^{-1} respectively. For the POGO method the size of the spatial sampling error is smaller, due to the smaller magnitude of the POGO velocities, which are averaged over 0–1000 m. The peak velocities from the POGO measurements are about a factor of three smaller than the 50–200 m averaged ADCP velocities. Based on this ratio, the estimated POGO sampling error is 1.2, 2.8, and 4.0 cm s^{-1} for CTD spacings of 20, 40, and 60 km, respectively.

The ageostrophic components of the velocity represent errors when a measured velocity is used for absolute referencing of a geostrophic shear profile, and this source of error affects all three of the referencing methods. Johns et al. (1989) have demonstrated that the largest component of the ageostrophic velocity in the Gulf Stream is the cyclostrophic term. Using current meter measurements from this experiment, the comparative sizes of the components of the ageostrophic velocity were tested, and the cyclostrophic contribution to the ageostrophic velocity was determined to be the largest for the NAC as well. Judging the radius of curvature of the NAC in this region is challenging, because satellite-derived maps of sea surface temperature are generally not available for this region due to an average 80–90% cloud cover (Peixoto and Oort, 1992). An estimate for the radius of curvature can be drawn from the radius of the Mann Eddy, a large, semi-permanent, anticyclonic eddy generally located just offshore of the NAC (Mann, 1967; Reiniger and Clarke, 1975; Clarke et al., 1980; Rossby, 1996). Since the Mann Eddy abuts the NAC on the offshore side, the radius of curvature of the NAC should be at least that large. Based on a large number of RAFOS float trajectories, Rossby (1996) has published a picture of the Newfoundland Basin region showing a radius for the Mann Eddy of about 140 km. Applying this value and a scale velocity of $U = 1$ m s^{-1}, the near surface cyclostrophic velocities are given by $U^2/fR = (1\ \mathrm{m\ s^{-1}})^2/(0.0001\ \mathrm{s^{-1}} \times 140000\ \mathrm{m}) = 7\ \mathrm{cm\ s^{-1}}$. This estimate is consistent with the current meter measurements, from which Meinen (1998) determined that the cyclostrophic velocity component at the shallowest current meter level, 400 m, had a standard deviation of about 7 cm s^{-1}. The magnitude of the cyclostrophic velocity observed by the POGO will be smaller due to the increased depth range. Using a scale velocity of 0.5 m s^{-1} for this increased depth range, the cyclostrophic velocities should be on the order of $U^2/fR = (0.5\ \mathrm{m\ s^{-1}})^2/(0.0001\ \mathrm{s^{-1}} \times 140000\ \mathrm{m}) = 2\ \mathrm{cm\ s^{-1}}$.

Table 1 lists the sizes of the errors to which each method is subject, each of which has been estimated using measurements obtained during this or concurrent

Table 1
Instrumental and oceanic errors of absolute reference velocities in the "ADCP btwn", "ADCP at", and POGO methods in cm s^{-1}. Columns for 20, 40, and 60 km refer to errors estimated for those station spacings. Errors that do not apply to particular methods are denoted by "n/a". For the environmental conditions and instrumental setup of this experiment the following sources combined to contribute less than 2 cm s^{-1} to the errors and were combined together as "Other" in the table; ADCP misalignment angle, GPS accuracy error, tides, Ekman velocities, scatter in the ADCP velocity measurement, ADCP amplitude coefficient error, and heading dependent gyrocompass error

Source of error	Bias or random	ADCP btwn	ADCP at 20/40/60 (km)	POGO 20/40/60 (km)
Spatial sampling error between CTD stations	Random	n/a	3.6/8.3/12.0	1.2/2.8/4.0
Curvature and other ageostrophic velocities	Random	7	7	2
Schuler oscillation	Random	5	0.9	n/a
Inertial oscillations	Random	2.5	2.5	1.8
Pogo velocity measurement	Random	n/a	n/a	1.9
Other	Random	1.9	1.9	0.1
	Bias	1.6	0.3	0.0

experiments. The size of many of these sources of error are dependent on the environmental conditions and instrumental setup of this experiment (e.g. low winds during the experiment produced low Ekman velocities as detailed in Meinen, 1998). The total error estimates for the "ADCP btwn", "ADCP at", and POGO reference velocities are biases of 1.6, 0.3, and 0.0 cm s^{-1} and standard deviations of 9.1, 11.3, and 4.4 cm s^{-1}, respectively (assuming a 40 km spacing for the "ADCP at" and POGO methods).

4. Results

Fig. 4A–D show the potential temperature (θ), salinity (S), potential density (σ_θ), and oxygen (O_2) sections from the CTD data. The NAC is evident, centered near 320 km in the section, identified by the large change in thermocline depth of about 700 dbars across the front. The sections also exhibit a core of very cold ($\theta < -1^\circ$C), very fresh ($S < 33.4$) water centered at about 75 km and 100 dbars, which is Labrador Current water that generally flows southward near the shelf-break. Also apparent in these sections are bowl-shaped isotherms and isohalines between 400 and 650 km, which characterize the Mann Eddy. There is also a hint of the deep Western Boundary Current at about 100 km near the 2500 m isobath in the θ and O_2 plots.

Fig. 5 shows the vertically averaged absolute velocity determined by each of the three referencing methods. The velocity structure is fairly consistent from method to method, with a few exceptions. Also shown are the associated error bars. The errors in the absolute geostrophic velocities were determined following the method described in Johns et al. (1989). Their method involves the quantification of the three types of error

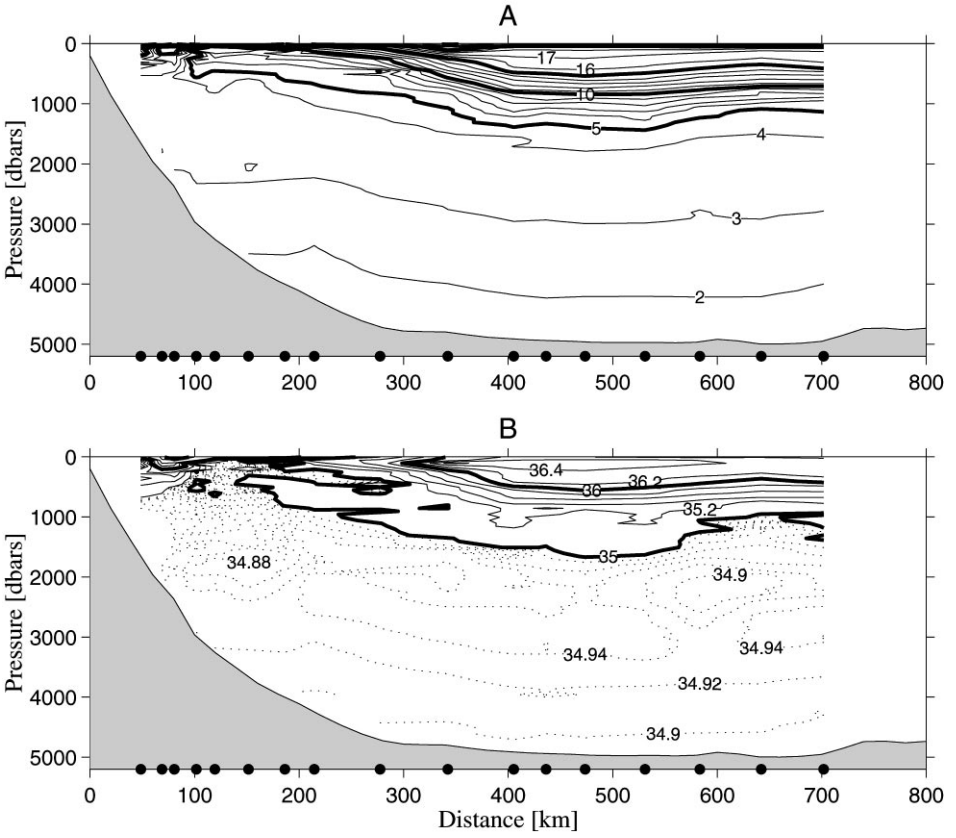

Fig. 4. Panels (A)–(D) show the potential temperature (°C), salinity, potential density relative to the surface (σ_θ), and oxygen (ml l^{-1}) sections across the NAC. Distance axis is measured from the 200 m isobath. Dark circles along lower axis denote the positions of CTD stations. Contour intervals are as follows: temperature contours are at 1°C intervals with bold contours every 5°C; salinity bold contours indicate intervals of 1, thin contours denote intervals of 0.2, and dotted contours indicate intervals of 0.02 (plotted only for contours below 35); density thin contours every 0.1 kg m^{-3} with bold contours every 0.5 kg m^{-3}; oxygen contour interval is 0.2 ml l^{-1} with bold contours every 1 ml l^{-1}.

in the calculation of geostrophic velocities: error in the geostrophically calculated geopotential heights; errors in the station locations; and errors in the absolute reference velocity. Because the "ADCP at" method produces the worst reference velocity accuracy it will no longer be discussed. With the geopotential heights determined to an accuracy of 0.04 m^2 s^{-2} (= 0.004 dyn m) (Johns et al., 1989), and station spacing accurate to about 1 km (a typical distance for the ship to move while approximately "on station" during a CTD cast), the total accuracy of the absolute geostrophic velocity profile for the POGO method is 5.2 cm s^{-1} (for a 50 km CTD spacing), and for the "ADCP btwn" method the absolute geostrophic velocities are

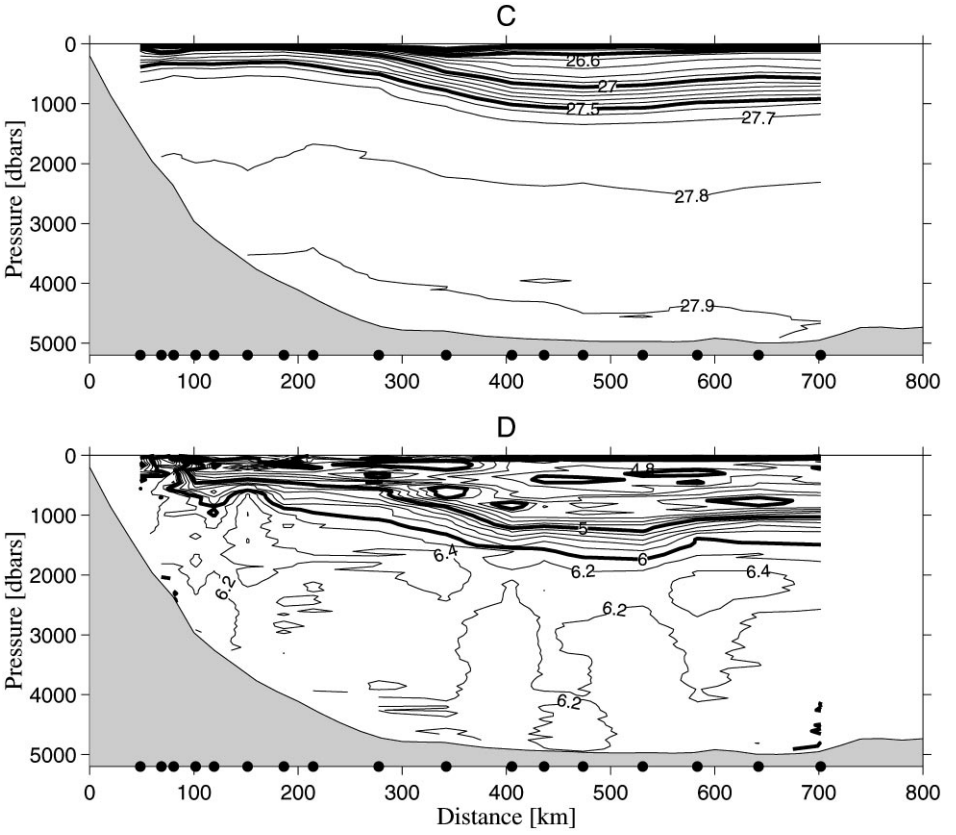

Fig. 4. (*continued*).

accurate to 9.2 cm s^{-1}. The POGO method, which has the smallest errors, was applied at all sites except those that lacked a POGO measurement at both CTD sites, due to the one POGO failure, and at one other site, where the ADCP measurements showed significant mesoscale structure between two CTD sites. At these sites the "ADCP btwn" method was used.

Fig. 6A shows the absolute velocity section referenced using the best available method. The main feature shown in the section is the baroclinic signature of the NAC, spanning 220–470 km and centered at about 320 km. Offshore of the NAC there is a considerable southward flow associated with the offshore edge of the Mann Eddy. The inshore edge of the Mann Eddy adds to the NAC to increase the northward transport. Inshore of the NAC are alternating bands of northward and southward flow including a strong southward flow just inshore of the NAC between 140 and 220 km. Fig. 6B plots the vertically averaged velocity section, similar to Fig. 5, with one standard deviation error bars. Examining the velocity structure shown in Fig. 6 in combination with the temperature, salinity, and oxygen data shown in Fig. 4 provides

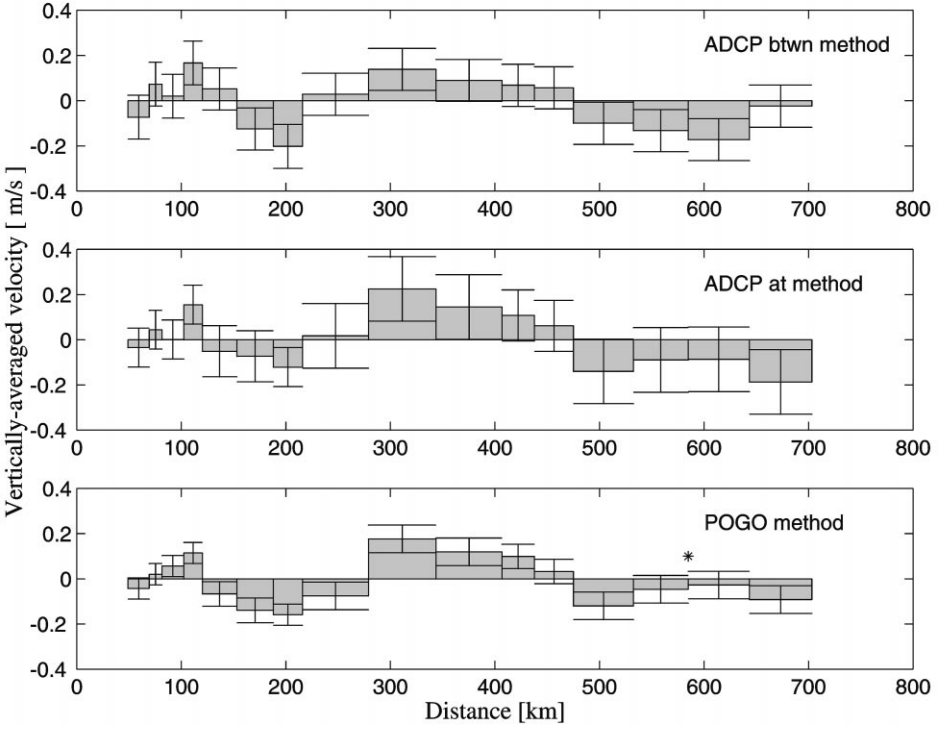

Fig. 5. The vertically averaged absolute velocity determined via three different referencing methods. The referencing method is noted in the upper right corner of each panel. Error bars indicate the accuracy of the calculated absolute velocities. Asterisk denotes location of failed POGO, "ADCP at" value used at that site.

information about the circulation at the time of this section. At the innermost edge of the section, part of the southward flowing Labrador Current is evident, identified by the very cold ($< 0^{\circ}C$) temperature and very fresh (< 34 psu) salinity signals. Between the Labrador Current and the northward flowing NAC in the mixed water regime is a band of northward velocity peaking at about $10\,cm\,s^{-1}$ and also a band of southward flow with a peak velocity of greater than $20\,cm\,s^{-1}$. The northward flowing waters are warmer and saltier than the southward flowing waters, suggestive of mixing processes south and north of the section. Offshore of the NAC, the southward flow within the offshore portion of the Mann Eddy appears. The northward flow within the inshore portion of the Mann Eddy has completely coalesced with the northward flow of the NAC, an effect commonly observed at this location in the past (Mountain and Shuhy, 1980; Clarke et al., 1980). The southward flow just inshore of the NAC is remarkable; this flow carries a southward transport of 58 Sv (1 Sverdrup [Sv] $= 10^6\,m^3\,s^{-1}$). The temperature ($\approx 3.5^{\circ}C$) and salinity (≈ 34.88) of the core of this water is consistent with that of Labrador Sea Water (LSW) (Tally and McCartney, 1982). However, the volume of this transport is quite surprising, being

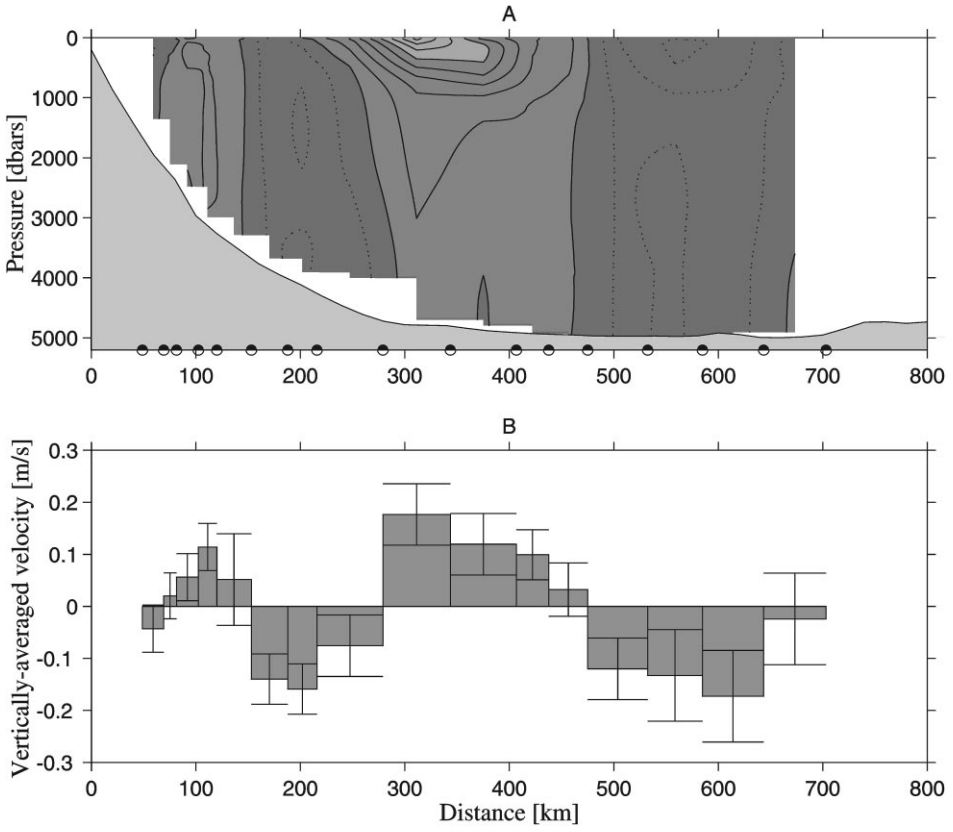

Fig. 6. Panel A – the absolutely referenced geostrophic velocity section, Panel B – the resulting vertically averaged velocity section, shown with one standard deviation error bars. On panel A, dark circles along the lower axis denote CTD stations. Dark gray shading indicates negative (southward) velocities, the medium gray indicates positive (northward) velocities in the range 0–50 cm s^{-1}, the light gray shading indicates positive velocity greater than 50 cm s^{-1}. Contour interval is 10 cm s^{-1}. Dotted contours indicate southward flow.

much larger than existing estimates of the entire southward flow of the Deep Western Boundary Current (Schmitz and McCartney, 1993). This indicates that there may be a significant recirculation inshore of the NAC at this location.

4.1. The transport of the NAC

The northward mass transport calculated for the NAC was 112 Sv. Note that the transport due to the inshore edge of the Mann Eddy, which also flows northward here, is included in this transport because there is no way to differentiate between the two northward flows. There are three sources of error in the transport calculation; station

spacing, geopotential height calculations, and error in the reference velocity. The station spacing and geopotential height errors in the geostrophic velocities are self-canceling from one CTD-pair to the next, because an error in station spacing or geopotential height will have opposite effects on the transport estimates from the CTD-pair to either side of the site. Across the full-width of the NAC (180 km), the geopotential height component of the velocity error is $\Delta v = \Delta\Phi/fL = 0.04\ \mathrm{m^2 s^{-2}}/(0.0001\ \mathrm{s^{-1}} \times 180000\ \mathrm{m}) = 0.2\ \mathrm{cm^{-1}}$; the velocity error due to inaccuracy in determining the station spacing is $\Delta v = (\delta L/L)\bar{v} = (1\ \mathrm{km}/180\ \mathrm{km}) \times 0.5\ \mathrm{m\ s^{-1}} = 0.3\ \mathrm{cm\ s^{-1}}$. The four CTD-pairs spanning the NAC provide 3 degrees of freedom, since neighboring gaps share a POGO, so the overall velocity error due to the reference velocity is reduced by $\sqrt{3}$. When the total velocity error for the absolute velocity section is multiplied by the average depth (4250 m) across the current and by the width of the current (180 km), the resulting transport accuracy for the NAC transport is $(\sqrt{(0.002\ \mathrm{m\ s^{-1}})^2 + (0.003\ \mathrm{m\ s^{-1}})^2 + (0.052\ \mathrm{m\ s^{-1}}/\sqrt{3})^2}) \times 4250\ \mathrm{m} \times 180000\ \mathrm{m} = 23$ Sv. The volume transport error arises primarily from the accuracy to which the absolute reference velocity is known.

The transport of 112 ± 23 Sv is consistent with the transport of 121 ± 50 Sv determined by three CTD shear velocity sections referenced by a line of current meters across the NAC over a few months in the early 1970s (Reiniger and Clarke 1975). This is the only previous absolute transport measurement for the NAC in this region. Reiniger and Clarke (1975) associated about 55S Sv of their 121 Sv with the circulation in the Mann Eddy, while they ascribed about 65 Sv to throughput transport. This is also the only estimate of the absolute transport of the Mann Eddy.

A number of transport estimates relative to a LNM at 2000 dbars or at the bottom have been made in this area. The transport of the NAC relative to a 2000 dbar LNM calculated using our section is 59 Sv. This is somewhat larger than the 44 Sv determined by Clarke et al. (1980) and the 35 Sv measured by Mann (1967). In the latter case, Mann was able to attribute transport separately to the NAC and the Mann Eddy, but they cannot be separated in our observations. Worthington (1976) presented two different realizations of the NAC + Mann Eddy northward transport calculated in this region relative to a LNM at the bottom, yielding 74 and 97 Sv. Using the same LNM, Clarke et al. (1980) obtain 78 Sv for their section. Our estimate relative to an LNM at the bottom, 91 Sv, falls between these estimates.

One key result from these measurements is an estimate of the component of the transport associated with the non-zero bottom velocity. The absolute transport can be decomposed into a baroclinic component relative to an LNM at the bottom, $\mathscr{T}_{\mathrm{relbtm}} = 91$ Sv, and a component associated with the bottom velocity extended through the whole water column, $\mathscr{T}_{\mathrm{btm}} = 21$ Sv. Without the absolute reference velocity measurements, the estimate of the NAC transport would be about 20% smaller than the actual absolute transport, $\mathscr{T}_{\mathrm{total}} = \mathscr{T}_{\mathrm{relbtm}} + \mathscr{T}_{\mathrm{btm}}$. This higher transport necessitates a future revision of the present understanding of the circulation in the Newfoundland Basin region to account for this larger transport.

5. Summary

Three different methods for determining the absolute velocity reference needed in the dynamic method have been used on a single hydrographic section across the North Atlantic Current completed in August, 1993. The three methods are: averaging the measurements of POGO transport floats taken at the two CTD sites; integrating the hull-mounted ADCP measurements between the two CTD sites; and averaging the time mean hull-mounted ADCP velocity measurements made at the two CTD sites. The method employing the POGO transport float has the smallest inherent errors for the three CTD spacings tested; 20, 40, and 60 km CTD spacings produce absolute geostrophic velocity accuracies of 4.8, 4.7, and 5.3 cm s^{-1} respectively. The primary reason the POGO errors are smaller is the lesser impact of ageostrophic velocities on the POGO measurements than on the measurements of the ADCP.

The transport of the North Atlantic Current at 42.5°N during the time period in which this section was taken is 112 ± 23 Sv. The large error bars are predominantly due to the ≈ 5 cm s^{-1} uncertainty in the absolute velocity reference. The accuracy of this transport estimate is considerably better, however, than the ± 50 Sv accuracy of the only previous absolute estimate of the North Atlantic Current in this region (Reiniger and Clarke, 1975). The component of the transport resulting from the non-zero bottom velocity represented about 20% of the total transport. Just inshore of the North Atlantic Current, 58 Sv flowed southward; the core of these waters had the T–S characteristics of Labrador Sea Water. The large magnitude of these flows indicates the circulation in the Newfoundland Basin may be much stronger than had previously been realized.

Acknowledgements

The authors would like to thank Karen Tracey, Sandy Fontana, and Mike Mulroney, who helped with the collection and initial processing of the CTD, ADCP, and POGO data. Thanks also to the officers and crew of the R.V. Oceanus for their work during the cruise. The POGO, ADCP, and CTDs were kindly provided by Dr. Tom Rossby at the University of Rhode Island. Funding for the current meter array was provided by the Bedford Institute of Oceanography, Department of Fisheries and Oceans, Halifax, Canada, and the Climate Greenplan Program of Environment Canada (Clarke). Funding for the Oceanus time and additional current meters was provided by the Office of Naval Research (Watts). A grant from the National Oceanic and Atmospheric Administration provided funds for analysis of the data (Watts). Finally, one author (Meinen) was funded during the early part of the experiment on an Office of Naval Research (Secretary of the Navy) graduate fellowship and completed his Ph.D. degree under funding from the National Oceanic and Atmospheric Administration.

References

RDI, 1989. Acoustic Doppler Current Profilers. Principles of Operation: A Practical Primer, RD Instruments, 36 pp.

Arhan, M., Colin de Verdiere, A., Mercier, H., 1989. Direct observations of the mean circulation at 48°N in the Atlantic Ocean. Journal of Physical Oceanography 19, 161–181.

Clarke, R.A., Hill, H.W., Reiniger, R.F., Warren, B.A., 1980. Current system south and east of the Grand Banks of Newfoundland. Journal of Physical Oceanography 10, 25–65.

Cokelet, E.D., Schall, M.L., Dougherty, D.M., 1996. ADCP-referenced geostrophic circulation in the Bering Sea Basin. Journal of Physical Oceanography 26, 1113–1128.

Fofonoff, N.P., Millard, R.C., 1983. Algorithms for computation of fundamental properties of seawater. Unesco Technical Papers in Marine Science, No. 44, 53 pp.

Gill, A.E., 1982. Atmosphere-Ocean Dynamics. Academic Press, New York.

Johns, E., Watts, D.R., Rossby, H.T., 1989. A Test of Geostrophy in the Gulf Stream. Journal of Geophysical Research 94 (C3), 3211–3222.

Joyce, T.M., Wunsch, C., Pierce, S.D., 1989. Synoptic Gulf Stream velocity profiles through simultaneous inversion of hydrographic and acoustic doppler data. Journal of Geophysical Research 91 (C6), 7573–7585.

Krauss, W.M., 1986. The North Atlantic Current. Journal of Geophysical Research 91, 5061–5074.

Mann, C.R., 1967. The termination of the Gulf Stream and the beginning of the North Atlantic Current. Deep Sea Research 14, 337–359.

McCartney, M.S., Talley, L.D., 1982. The subpolar mode water of the North Atlantic ocean. Journal of Physical Oceanography 12, 1169–1188.

McCartney, M.S., Talley, L.D., 1984. Warm-to-cold water conversion in the northern North Atlantic ocean. Journal of Physical Oceanography 14 (5), 922–935.

Meinen, C.S., 1998. Transport of the North Atlantic Current. Ph.D. Thesis, University of Rhode Island.

Mountain, D.G., Shuhy, J.L., 1980. Circulation near the Newfoundland Ridge. Journal of Marine Research 38, 205–213.

Peixoto, J.P., Oort, A.H., 1992. Physics of Climate. AIP Press, New York.

Pickart, R.S., Lindstrom, S.S., 1994. A comparison of techniques for referencing geostrophic velocities. Journal of Atmospheric Oceanic Technology 11, 814–824.

Pollard, R., Read, J., 1989. A Method for calibrating shipmounted Acoustic Doppler Profilers and the limitations of Gyro Compasses. Journal of Atmospheric Oceanic Technology 6 (6), 859–865.

Pond, S., Pickard, G.L., 1983. Introductory Dynamical Oceanography 2nd Edition. Pergamon Press, Oxford.

Reiniger, R.F., Clarke, R.A., 1975. Circulation pattern in the Newfoundland ridge area. 1972. Special Publication 10, pages International Commission for the Northwest Atlantic Fisheries, Dartmouth Canada, pp. 57–67.

Rossby, T., 1996. The North Atlantic Current and surrounding waters: At the Crossroads. Review of Geophysics 34 (4), 463–481.

Rossby, T., Fontaine, J., Hummon, J., 1991. Measuring mean velocities with POGO. Journal of Atmospheric Oceanic Technology 8, 713–717.

Saunders, P.M., King, B.A., 1995. Bottom currents derived from a shipborne ADCP on WOCE cruise A11 in the South Atlantic. Journal of Physical Oceanology 25, 329–347.

Schmitz Jr., W.J., McCartney, M.S., 1993. On the North Atlantic circulation. Review of Geophysics 31, 29–49.

Sy, A., Schauer, U., Meincke, J., 1992. The North Atlantic Current and its associated hydrographic structure above and eastwards of the Mid-Atlantic Ridge. Deep Sea Research 39 (5), 825–853.

Tally, L.D., McCartney, M.S., 1982. Distribution and circulation of Labrador Sea Water. Journal of Physical Oceanography 12, 1189–1205.

Worthington, L.V., 1976. On the North Atlantic Circulation. The Johns Hopkins Oceanographic Studies, Number 6. The Johns Hopkins University Press, Baltimore, MD.